Quantum spin fluctuations in dynamical quantum phase transitions

Cheuk Yiu Wong [1], Hadi Cheraghi [2], and Wing Chi Yu [1,*]

[1] *Department of Physics, City University of Hong Kong, Kowloon, Hong Kong*
[2] *Institute of Physics, Maria Curie-Skłodowska University, 20-031 Lublin, Poland*

Quantum phase transitions have long been studied in their relation to quantum fluctuations. These fluctuations can be quantified as the degree of spin squeezing in spin models, where one of the two noncommutative observables breaks the standard quantum limit of measurement by minimizing its uncertainty. However, the understanding of their role in dynamical quantum phase transitions (DQPTs) is still incomplete. In this work, we combine the Loschmidt amplitude, which detects DQPTs, and the spin-squeezing parameter (SSP), the quantification of spin squeezing, to study the spin dynamics in a quenched interacting spin model around DQPT. We show that the extremum, mostly maximum, of SSP occurs near DQPTs when the system is quenched between different phases. These phenomena further unveil the spin correlations during DQPTs, for which the highest contribution aligns with the preferred direction of spin interactions in the postquenched phase. We also demonstrate that the time evolution of SSP differs for various quench scenarios. These findings provide us with physical insights into the dynamics of quantum fluctuations around DQPTs and their relation to the equilibrium phase diagrams.

I. INTRODUCTION

Dynamical quantum phase transitions (DQPTs) have been serving as a theoretical framework on far-from-equilibrium physics of quantum many-body systems. The theory originates as an analogy to the equilibrium statistical mechanics about the phase transitions [1–3]. DQPTs can be triggered through a sudden quench protocol from the initially prepared Hamiltonian H_i in one phase or at phase boundary to the final Hamiltonian H_f in another phase. DQPTs occur at times when the dynamic quantity the Loschmidt amplitude (LA), defined as

$$\mathcal{G}(t) = \langle \psi_0^i | \psi(t) \rangle = \langle \psi_0^i | e^{-iH_f t/\hbar} | \psi_0^i \rangle, \quad (1)$$

the overlap of the time-evolved state $|\psi(t)\rangle$ onto the initial ground state $|\psi_0^i\rangle$, vanishes, or equivalently the dynamic free energy or Loschmidt rate (LR)

$$\lambda(t) = -\lim_{N \to \infty} \frac{1}{N} \ln[\mathcal{L}(t)], \quad (2)$$

where $\mathcal{L}(t) = |\mathcal{G}(t)|^2$ is termed the Loschmidt echo (LE), behaves nonanalytically [1–3]. This is the definition of type-II DQPTs. On the other hand, the type-I DQPT is defined under the long-term dynamics of a system's order parameter on a sudden quench [4–8]. Supported by the realization of DQPTs in experiments for various quantum systems via quantum simulators [9–18], the establishment of the DQPT theories thrives. There has been research on the fundamental properties of DQPTs and the theoretical studies of DQPTs in various quantum models [1–8,19–72]. DQPTs are also substantially

shown to have deep connections to the entanglement spectrum and correlation matrix [2,26–31,46,68].

The wealth of linkage to the entanglement motivates the investigation of a more experimentally accessible quantity regarding spin dynamics, the *spin-squeezing parameter* (SSP). The SSP quantifies the quantum fluctuation when one measures one of two noncommutative spin observables and it has various definitions fitting the purpose of studies [73–75]. The idea of using SSP as a tool to study quantum phase transitions was introduced in the past twenty years [76–78]. A recent paper showed that a certain definition of SSP can be a probe to detect the type-I DQPT, where the SSP behaves nonanalytically against the tunable parameter of a Bose-Einstein condensate after a sudden quench across a certain phase boundary [79]. A similar effect is also observed in experiment for another model between different dynamical phases [16]. A recent work on SSP in the one-dimensional (1D) XY model, where the authors showed the possibility to generate the spin-squeezed state from an originally unsqueezed system by quenching, also stated the nonanalyticities found in long-time-averaged SSP against the postquenched Hamiltonian for an arbitrary prequenched Hamiltonian, and suggested a potential linkage to equilibrium phase transitions [80]. These works seem to suggest a potential connection between type-I DQPTs and quantum fluctuations, while the short-term physical nature behind the type-II DQPTs is not well addressed.

Inspired by the extensive use of spin squeezing in the mentioned research, we investigate the spin dynamics by observing the spin squeezing of a spin-$\frac{1}{2}$ model around DQPTs under different quench protocols in this work. We adopt the definition of SSP by Ueda and Kitagawa [81],

$$\xi_S^2 = \frac{4(\Delta J_{\hat{n}_\perp})^2}{N}, \quad (3)$$

*wingcyu@cityu.edu.hk

where $(\Delta J_{\hat{n}_\perp})^2$ denotes the variance of the spin operators orthogonal to the mean-spin direction (MSD) of the system, with the spin operators defined as

$$J_a = \frac{1}{2} \sum_{j=1}^{N} \sigma_j^a, \quad a = x, y, z. \tag{4}$$

The state is considered to be squeezed if $\xi_S^2 < 1$, and the larger the SSP is, the less the state is squeezed.

In this work, we combine the conventional LA analysis under a sudden quench and the study of time evolution of SSP defined by Eq. (3) in the XY model. Along with extracting explicitly the two-point correlation functions in the analytical expression of SSP, we demonstrate how the evolution of quantum fluctuation unveils the spin correlations during DQPT. Namely, our results show the SSP attains local maximum near DQPT in most of the cases. Furthermore, we show the cause of this increase aligns with the physical properties of the underlying equilibrium phase the system is quenched to. We also distinguish the evolution pattern of SSP for different types of quench, namely quenches across and from the equilibrium phase boundary, and within one phase, in the regime around the first critical time. We believe our study provides insights on filling the knowledge gap of spin fluctuation in DQPTs as well as the physical essence of DQPTs.

The paper is organized as follows: Section II covers the analytical details necessary for the study, including the expression of LA and SSP. Section III demonstrates the findings in different quench scenarios, with subsections divided as follows: Section III A contains the analysis on quenches between Ising ferromagnetic (FM) and paramagnetic (PM) phases, Sec. III B analyzes the results for quenches between anisotropic phases, and Sec. III C is the analysis of quenches from the multicritical point of the XY model. Finally, a conclusion and some future perspectives regarding this work are given in the last section.

II. FORMULATION AND 1D XY MODEL

We demonstrate our analysis on the 1D XY model which is an integrable model and has proven the existence of DQPTs [38,69]. The Hamiltonian is the following,

$$H(\delta, g) = -\frac{\hbar}{2} \sum_{j=1}^{N} \left[J \left(\frac{1+\delta}{2} \sigma_j^x \sigma_{j+1}^x + \frac{1-\delta}{2} \sigma_j^y \sigma_{j+1}^y \right) + g \sigma_j^z \right], \tag{5}$$

where N specifies the system size, J is the coupling strength, δ governs the anisotropic coupling between spins along the x and y directions, g is the external magnetic field strength along the z direction, and the periodic boundary condition is adopted. Below we set $\hbar = J = 1$ for convenience. The model exhibits competitions between anisotropic and magnetic coupling which results in the existence of multiple phases. In particular, $g < 1$ gives rise to the FM phase, where it is further divided into the x-spin dominant FM_x phase and y-spin dominant FM_y phase depending on the sign of δ. When $g > 1$, the model transits to the PM phase with the ground-state MSD aligning parallel to the external magnetic field. Figure 1 shows the equilibrium phase diagram of the 1D XY model. We will
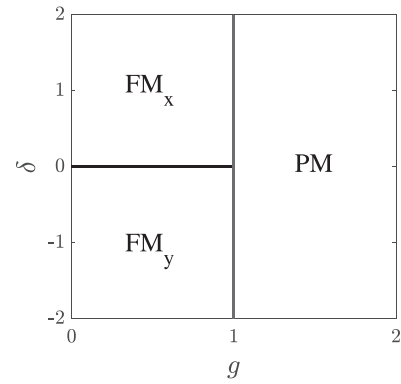

FIG. 1. Schematic drawing of the ground-state phase diagram of the equilibrium 1D XY model.

perform quenches across and from different phase boundaries and critical points.

We study the quench dynamics of the model by first performing Jordan-Wigner transformation $\sigma_j^+ = \exp[i\pi \sum_{l<j} c_l^\dagger c_l] c_j$ and $\sigma_j^z = 1 - 2c_j^\dagger c_j$, followed by a Fourier transformation $c_j = (1/\sqrt{N}) \sum_k e^{-ijk} c_k$ [82–84], and turn the Hamiltonian into

$$H(\delta, g) = \sum_{k>0} \eta_k^\dagger H(k) \eta_k, \tag{6}$$

where $\eta_k = (c_k, c_{-k}^\dagger)^T$ and $H(k) = \vec{d}(k) \cdot \vec{\sigma}$ is the Bloch Hamiltonian with the Bloch vector $\vec{d}(k) = (0, -\delta \sin k, g - \cos k)^T$ and $\vec{\sigma} = (\sigma^x, \sigma^y, \sigma^z)$ are the Pauli matrices [35]. For the sake of analysis, we concern the unit Bloch vectors $\hat{d}(k) = \vec{d}(k)/|\vec{d}(k)|$. We restrict our calculations to the even-parity subspace and N is even with the k's of the form $k = (2m - 1)\pi/N$, where $m = 1, 2, \ldots, N/2$. Performing the Bogoliubov transformation $c_k = \cos[\theta_k(\delta, g)]\beta_k + i \sin[\theta_k(\delta, g)]\beta_{-k}^\dagger$, the diagonalized Hamiltonian reads

$$H(\delta, g) = \sum_{k>0} \varepsilon_k(\delta, g)(\beta_k^\dagger \beta_k - \beta_{-k}\beta_{-k}^\dagger), \tag{7}$$

where $\varepsilon_k(\delta, g) = |\vec{d}(k)| = \sqrt{(\cos k - g)^2 + (\delta \sin k)^2}$ is the quasiparticle eigenenergy, and $\theta_k(\delta, g) \in [0, \pi/2]$ is the Bogoliubov angle defined such that $\tan[2\theta_k(\delta, g)] \equiv \delta \sin k/(\cos k - g)$.

Consider the system initially prepared in $H_i = H(\delta_i, g_i)$ and quenched to $H_f = H(\delta_f, g_f)$. Using the vacuum state as the initial state, LA in Eq. (1) can be decomposed into momentum-wise form, namely $\mathcal{G}(t) = \prod_{k>0} \mathcal{G}_k(t)$, where

$$\mathcal{G}_k(t) = \cos^2 \phi_k e^{i\varepsilon_k(\delta_f, g_f)t} + \sin^2 \phi_k e^{-i\varepsilon_k(\delta_f, g_f)t} \tag{8}$$

with $\phi_k = \theta_k^i - \theta_k^f$ being the difference between the initial and the final Bogoliubov angles. The nonanalyticities in LA occur when $\phi_k = \pm\pi/4$ at critical times

$$t_c^p = \frac{\pi}{\varepsilon_{k^*}^f} \left(p - \frac{1}{2} \right), \quad p \in \mathbb{N}, \tag{9}$$

where k^* is the *critical momentum* when the corresponding initial and final unit Bloch vectors $\hat{d}_i(k^*)$ and $\hat{d}_f(k^*)$ are orthogonal to each other, i.e., $\hat{d}_i(k^*) \cdot \hat{d}_f(k^*) = 0$.

The behavior of the momentum-wise LA can be visualized by the vector introduced by Ding [52]:

$$\vec{r}_k(t) = (x_k, y_k) = |\mathcal{G}_k(t)| e^{i\phi_k^G(t)}, \tag{10}$$

where $\phi_k^G(t) = \phi_k^{\mathcal{G}}(t) - \phi_k^{\text{dyn}}(t)$ is the Pancharactnam geometric phase (PGP) [85,86], defined by the difference between the phase of LA $\phi_k^{\mathcal{G}}(t) = \text{Arg}[\mathcal{G}_k(t)]$ and the dynamical phase $\phi_k^{\text{dyn}}(t) = -\int_0^t dt' \langle\psi_k(t')|H_f(k)|\psi_k(t')\rangle = \varepsilon_k^f \cos(2\phi_k)t$. The PGP characterizes the dynamical topological order parameter (DTOP) [35]

$$\nu_D = \frac{1}{2\pi} \oint_0^\pi \frac{\partial \phi_k^G(t)}{\partial k}, \tag{11}$$

which changes its value at DQPTs.

On the other hand, we adopt the formulation in Ref. [80] regarding the spin dynamics analysis. The MSD of the XY model is along the z direction as a result of the $\mathbb{Z}_2$ symmetry which guarantees $\langle J_x\rangle = \langle J_y\rangle = 0$. The factor $(\Delta J_{\hat{n}_\perp})^2$ in Eq. (3) is then taken to be $[(\cos\alpha)J_x + (\sin\alpha)J_y]^2$. Setting $\langle\mathcal{O}\rangle \equiv \langle\psi(t)|\mathcal{O}|\psi(t)\rangle$ for any operator $\mathcal{O}$ for simplicity, the SSP reads

$$\xi_S^2(t) = \frac{2}{N} \min\left\{\langle J_x^2 + J_y^2\rangle + J(\alpha, t)\right\}, \tag{12}$$

where

$$J(\alpha, t) = \cos(2\alpha)\langle J_x^2 - J_y^2\rangle + \sin(2\alpha)\langle J_xJ_y + J_yJ_x\rangle. \tag{13}$$

The angle which yields the minimum of Eq. (12) is termed the *squeezing angle* and is denoted as α_s in the following. This quantity has been studied in the context of qubit systems relating its time evolution to the energy spectrum of the systems [87]. In this paper, we will demonstrate how it embeds the

competition between the net parallel-spin contribution and the cross-spin contribution over time. With transitional symmetry of the chain, the time evolution of SSP can be written as

$$\xi_S^2(t) = 1 + 2\sum_{n=1}^{N-1}\left[G_n^{xx}(t) + G_n^{yy}(t)\right]$$
$$- 2\left\{\left[\sum_{n=1}^{N-1}\left[G_n^{xx}(t) - G_n^{yy}(t)\right]\right]^2 \right.$$
$$\left. + \left[\sum_{n=1}^{N-1}\left[G_n^{xy}(t) + G_n^{yx}(t)\right]\right]^2\right\}^{\frac{1}{2}}, \tag{14}$$

where $G_n^{ab}(t) = \langle\sigma_1^a\sigma_{1+n}^b\rangle/4$ is the correlation function along directions a and b and $G_0^{aa}(t) = \langle\sigma_1^a\sigma_1^a\rangle/4 = 1/4$.

The calculation of the correlation functions involves computing strings of operators of the forms [88]

$$G_n^{xx}(t) = \frac{1}{4}\langle B_1A_2B_2\cdots A_nB_nA_{n+1}\rangle,$$
$$G_n^{yy}(t) = \frac{(-1)^n}{4}\langle A_1B_2A_2\cdots B_nA_nB_{n+1}\rangle,$$
$$G_n^{xy}(t) = \frac{i}{4}\langle B_1A_2B_2\cdots A_nB_nB_{n+1}\rangle, \tag{15}$$
$$G_n^{yx}(t) = \frac{i(-1)^{n-1}}{4}\langle A_1B_2A_2\cdots B_nA_nA_{n+1}\rangle,$$

where $A = c_j^\dagger + c_j$ and $B = c_j^\dagger - c_j$ in the Jordan-Wigner basis. By Wick's theorem, the expectation values turn into sums of all possible permutations of products of operator pairs, which turns out to be a problem of calculating Pfaffians of $2n \times 2n$ skew-symmetric matrices

$$G_n^{ab}(t) \sim \text{Pf}\begin{pmatrix} \langle\mathcal{O}_1\mathcal{O}_2\rangle & \langle\mathcal{O}_1\mathcal{O}_3\rangle & \langle\mathcal{O}_1\mathcal{O}_4\rangle & \cdots & \langle\mathcal{O}_1\mathcal{O}_{2n}\rangle \\ & \langle\mathcal{O}_2\mathcal{O}_3\rangle & \langle\mathcal{O}_2\mathcal{O}_4\rangle & \cdots & \langle\mathcal{O}_2\mathcal{O}_{2n}\rangle \\ & & \langle\mathcal{O}_3\mathcal{O}_4\rangle & \cdots & \langle\mathcal{O}_3\mathcal{O}_{2n}\rangle \\ & & & \ddots & \vdots \\ & & & & \langle\mathcal{O}_{2n-1}\mathcal{O}_{2n}\rangle \end{pmatrix}. \tag{16}$$

Note that at $t = 0$ for parallel-spin correlation $a = b = x, y$, the Pfaffians reduce to Toeplitz determinants known for the analytical works of Lieb *et al.* in correlation function calculations in the XY model [88]. The elements of the Pfaffians are four types of two-point functions as follows:

$$\langle A_jA_{j+n}\rangle = \langle B_jB_{j+n}\rangle$$
$$= -i\frac{2}{N}\sum_{k>0}\sin(2\phi_k)\sin(nk)\sin(2\varepsilon_k^f t),$$
$$\langle A_jB_{j+n}\rangle = \frac{2}{N}\sum_{k>0}\left[\cos(2\phi_k)\cos(2\theta_k^f + nk)\right.$$
$$\left. - \sin(2\phi_k)\sin(2\theta_k^f + nk)\cos(2\varepsilon_k^f t)\right],$$
$$\langle B_jA_{j+n}\rangle = -\frac{2}{N}\sum_{k>0}\left[\cos(2\phi_k)\cos(2\theta_k^f - nk)\right.$$
$$\left. - \sin(2\phi_k)\sin(2\theta_k^f - nk)\cos(2\varepsilon_k^f t)\right]. \tag{17}$$

In the next section, we study the spin dynamics in terms of the SSP and the correlation functions in relation to DQPT under three scenarios:

(1) quenches between Ising phases, where we fix the δ and alter along g;

(2) quenches between anisotropic phases, where we fixed g and quench along δ in the region bounded by $-\infty < \delta < \infty$ and $0 \leqslant g < 1$;

(3) quenches from the multicritical point $(\delta_c, g_c) = (0, 1)$.

Alternatively we use the shorthand notation $(\delta_i, g_i) \to (\delta_f, g_f)$ for any quench when necessary. All quenches were performed on an $N = 100$ system, and we concentrate our discussion around the first critical time.

III. DYNAMICS OF SPIN SQUEEZING

A. Quenches between Ising phases

We performed quench cases involving the Ising boundary $g_c = 1$ while fixing $\delta = 0.8$. The quench dynamics of forward
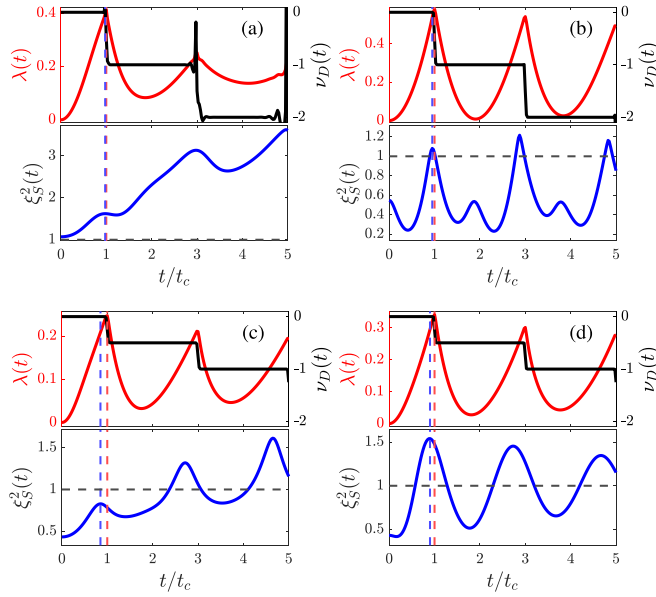
FIG. 2. Scaled time plots of LR, DTOP (top panels), and SSP (bottom panels) at $\delta = 0.8$ for (a) $g_i = 0.4 \to g_f = 2$, (b) $g_i = 2 \to g_f = 0.1$, (c) $g_i = 1 \to g_f = 2$, and (d) $g_i = 1 \to g_f = 0.5$. Red and blue dashed lines indicate the first peak of LRs and SSPs, respectively. Black dashed horizontal lines indicate $\xi_S^2(t) = 1$.

FIG. 3. Trajectories of $\vec{r}_k$'s at the corresponding critical times for the same quench cases as in Fig. 2. Black dots indicate the origin at which the vectors are located. The color scale shows the progression of $\vec{r}_k$'s from $k = 0$ to π.

quench ($g_i < g_f$), backward quench ($g_i > g_f$), and quench from the critical point ($g_i = g_c = 1$) are shown in Fig. 2. The DTOPs show the discontinuous jumps at critical times as expected. Note that all the extra spikes on the DTOPs in this paper are finite-size effects as confirmed numerically and they would vanish to give the true DTOP evolution pattern shown in Ref. [35] for larger systems. The vectors $\vec{r}_k$ plotted in Figs. 3(a) and 3(b) swipe a full circle passing through the origin for quenches across the equilibrium phase boundary. The momentum at which the vector is zero is the critical momentum, where $\mathcal{G}_{k^*}(t_c) = 0$. $\vec{r}_k$'s only swipe half a circle for quenches from the critical point, which is consistent with the observation in Ref. [52], and this leads to the half-integer jump in DTOP.

From Fig. 2, we observe that the peaks of SSPs in whichever case occur slightly sooner than the DQPTs. Note that the critical times indicated in the figures are calculated by Eq. (9) in the thermodynamic limit. For system sizes $N \geqslant 100$, the peak times extracted from SSP do not change significantly, suggesting this time discrepancy remains in larger systems. Nevertheless, the SSP is a local maximum, which implies that the state is the least spin-squeezed, in the vicinity of DQPT. The difference between forward and backward quenches is that the SSP keeps increasing for forward quenches (left column of Fig. 2) while it stays near and below 1 for backward quenches (right column of Fig. 2), but they both have some revival effects during DQPT where the spin-squeezing parameter falls following its peak, decreasing in parallel to the Loschmidt rate. This suggests that the system is around its most uncertain spin state along the direction perpendicular to the MSD around the critical time.

The evolution pattern of SSPs can be qualitatively understood via the summed time-evolved correlation functions
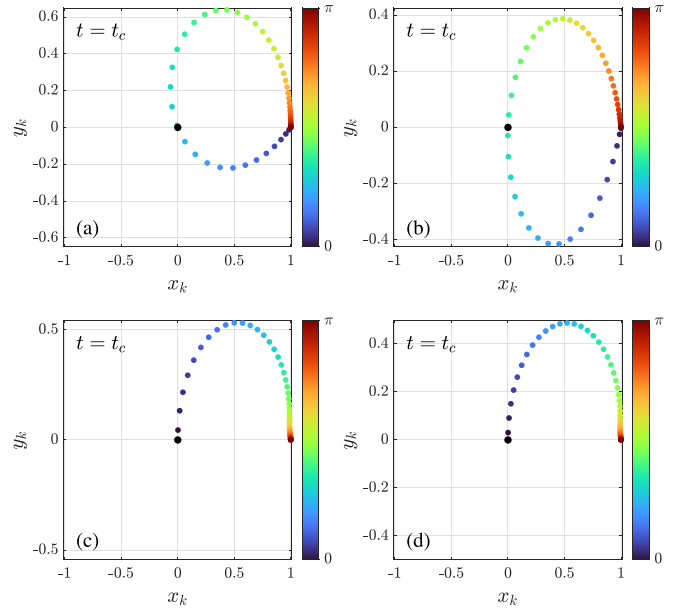
and squeezing angle, which are plotted in Figs. 4 and 5, respectively. For forward quenches including quenches from the Ising boundary [Figs. 4(a) and 4(c)], the x-direction correlation dominates initially as expected. As one approaches the first critical time, the y-direction correlation functions surpass the x-direction correlations. At the same time, the effect of cross-direction correlations $G_n^{\text{cross}}(t) = G_n^{xy}(t) + G_n^{yx}(t)$ grows rapidly. In the vicinity of the first DQPT, this surpassing effect is among the highest while the contribution from the cross-direction correlations sinks to near zero. After the DQPT, $G_n^{xx}(t)$'s revive partly, and both $G_n^{xx}(t)$'s and $G_n^{yy}(t)$'s have small but nonzero contributions while the cross-spin correlations oscillate around zero in the later time. This phenomenon resonates with the fact that the quench is from the FM phase, which is xx-correlation dominant, to the PM phase, in which none of the x and y correlations dominate. Around DQPT, the system not only stays temporarily least spin-squeezed, but also the farthest away from the original phase where yy correlations thrive and surpass xx correlations.

In terms of the squeezing angle, we see from Eq. (13) that $J(\alpha_s, t)$ exhibits dynamics resembling the rotation of a vector during quenching. In particular, we define a *squeezing vector* with x component $\langle J_x^2 - J_y^2 \rangle$ and y component $\langle J_x J_y + J_y J_x \rangle$ and an angle $2\alpha_s$ between them. By observing the evolution of the squeezing angle α_s as indicated by the gray dots in the plots, the vector has "rotated" in the clockwise direction for about half a circle before reaching the first critical time. The change of α_s seems to be the most rapid across DQPT. After one revival of the LE where the LR attains a local minimum (at $t/t_c \approx 2$), the vector has completed about a full revolution.

On the other hand, from Figs. 4(b) and 4(d), backward quenches seem to align with our observation to the spin nature of the system established before: The correlation functions along the x direction are the strongest alongside with a local
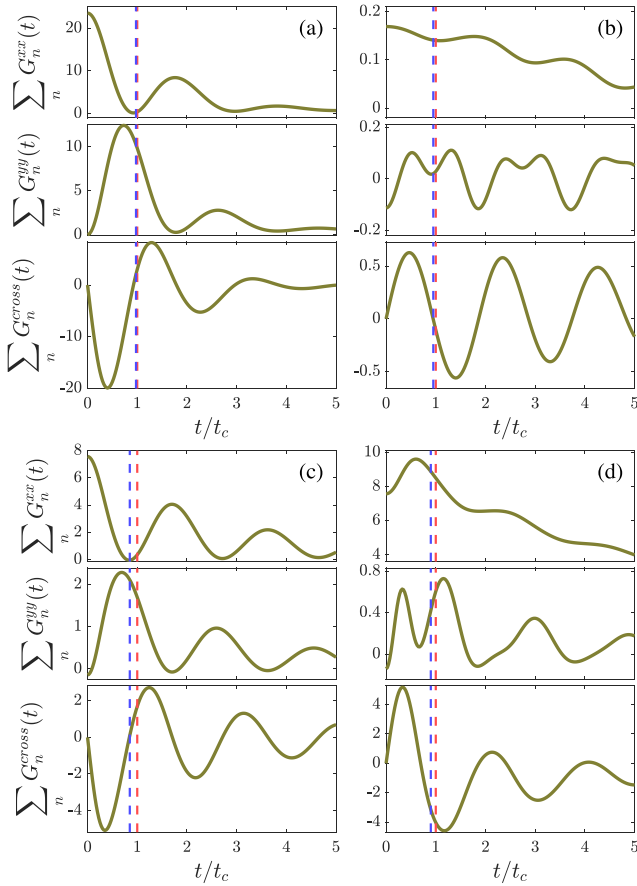
FIG. 4. Scaled time plots of sums of correlation functions $G_n^{xx}(t)$ (top panels), $G_n^{yy}(t)$ (middle panels), and $G_n^{cross}(t)$ (bottom panels) for the same quench cases as in Fig. 2. Red and blue dashed lines indicate the first peak of LRs and SSPs, respectively.

minimum of y-direction correlations in the vicinity of DQPT, marking the temporary transition to a state with FM$_x$ character. Apart from that, the contribution from the cross-spin correlations briefly vanishes. In fact, in all quenches except those from the Ising boundary the $G_n^{cross}(t)$'s change their sign when passing the critical time. The sign change is opposite to that for forward quenches. Another qualitative difference from forward quenches is the rotation direction of the squeezing vector, where it rotates anticlockwise initially and the motion oscillates around $\alpha = \pi/2$ [see Figs. 5(b) and 5(d)]. Like the forward quenches, the rate of change of α_s around DQPT is the strongest and the features are more apparent for "longer" ($\Delta g = g_f - g_i$ is large) quenches.

B. Quenches between anisotropic phases

The dynamics of the system in quenches between the anisotropic phases behaves differently from that between Ising phases. One major difference is that there will be two critical momenta k_1^* and k_2^* whenever one quenches across the anisotropic boundary, which in turn give two critical times $t_{c,1}$ and $t_{c,2}$. Budich and Heyl showed that at the two critical momenta, the Bloch vectors rotate in opposite direction when passing through the respective critical time [35]. Here we demonstrate this idea through the vector defined in Eq. (10)
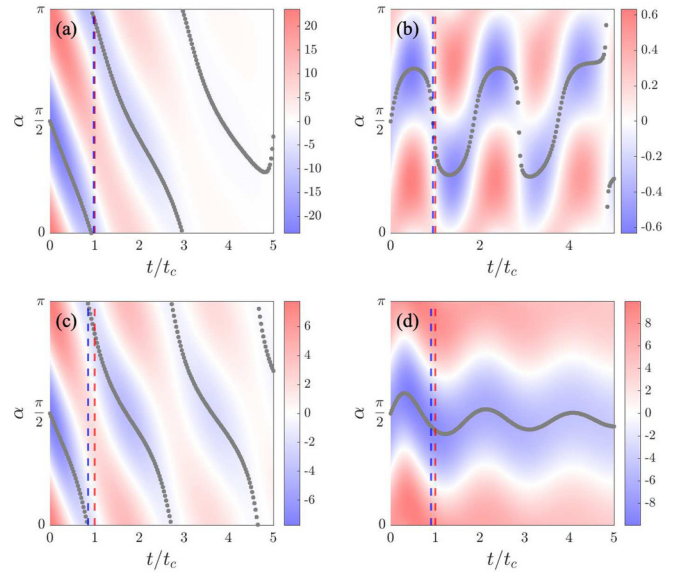

FIG. 5. Color map of $J(\alpha, t)$ for the same quench as in Fig. 2. Gray dots emphasize the squeezing angle α_s. Red and blue dashed lines refer to the first peak of LRs and SSPs, respectively.

and further explore the system's dynamics through the spin-squeezing parameter.

The anisotropic boundary is at $\delta_c = 0$, separating two phases: the x-spin dominant FM$_x$ phase ($\delta > 0$) and the y-spin dominant FM$_y$ phase ($\delta < 0$). We fix g to 0.5 and quench from FM$_y$ to FM$_x$ phase (upward quench), FM$_x$ to FM$_y$ phase (downward quench), and also from the equilibrium phase boundary. Their dynamics are shown in Fig. 6. Clearly from the DTOPs in Figs. 6(a) and 6(b), we can observe the negative and positive jumps at $t_{c,1}$ and $t_{c,2}$, respectively. For each critical time, there is an SSP peak slightly before it, which is the same as those quenches in the case involving the Ising phases in Sec. III A. Notice that the upward and downward quenches are similar for a fixed g, unlike the forward and backward quenches in Ising scenarios.

The existence of two critical momenta can be realized in the trajectory of $\vec{r}_k$. Namely, there are two "loops" in the trajectory plot. At whichever critical time, the corresponding vector $\vec{r}_{k^*}$ vanishes. Figures 7(a) and 7(b) demonstrate the phenomena at $t_{c,1}$, the critical time for k_1^*. When the system keeps evolving, the blue loop would expand further and it touches the origin at $t_{c,2}$, the critical time for k_2^* [as shown in Figs. 7(c) and 7(d)]. The opposite circular motion of the trajectories provides a visualization of the integer jumps in DTOP when passing through critical times.

On the other hand, the dynamics of quench from the anisotropic boundary is qualitatively very different from other quenches. The DTOP does not behave as expected [see the top panels of Figs. 6(c) and 6(d)]; it has nonanalyticities at critical times, yet it does not jump between adjacent DQPTs. This can be seen by the $\vec{r}_k$ in Figs. 7(e) and 7(f), where the trajectory does not change smoothly at DQPT when crossing the critical momentum, but the angles do. The evolution of SSP goes from a very high value to a minimum around DQPT. Unlike other quench scenarios, the system is among the most squeezed state near DQPT. The cause of this might be that
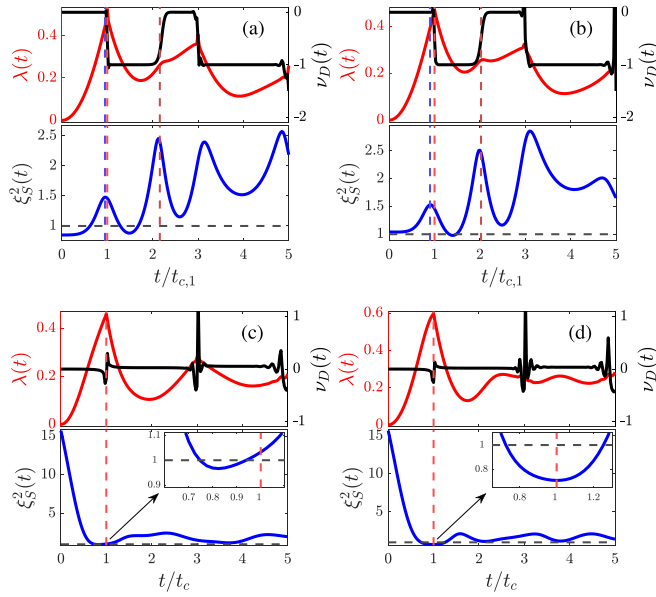
FIG. 6. Scaled time plots of LR, DTOP (top panels), and SSP (bottom panels) at $g = 0.5$ for (a) $\delta_i = -1.2 \rightarrow \delta_f = 0.8$, (b) $\delta_i = 0.8 \rightarrow \delta_f = -0.8$, (c) $\delta_i = 0 \rightarrow \delta_f = 0.8$, and (d) $\delta_i = 0 \rightarrow \delta_f = -1.2$. Red and blue dashed lines indicate the first peak of LRs and SSPs, respectively. The second red dashed lines in (a) and (b) represent the second critical time $t_{c,2}$ for each quench. Black dashed horizontal lines indicate $\xi_S^2(t) = 1$. The inset plots in (c) and (d) display the zoomed SSP around the first critical time.

the equilibrium SSP in the domain $\delta = 0$, $g \in [0, 1)$ diverges. When quenched out of the phase boundary, the SSP falls rapidly and reaches its minimum near DQPT.

Since anisotropic phases involves competition between x- and y-spin interactions, a more direct interpretation about what is happening during DQPT via the time evolution of the summed correlation functions can be observed in Fig. 8. In particular, the upward quenches in Fig. 8(a) do show an increase in $G_n^{xx}(t)$ and a decrease in $G_n^{yy}(t)$, and they reach maximum and minimum, respectively, in the vicinity of the first DQPT. The downward quenches in Fig. 8(b) show the opposite phenomenon. In both cases, the contribution of cross-spin correlations vanishes at the first critical times. One observes the same effect for quenches from the anisotropic boundary, where the xx correlations reach a higher value while yy correlations drop to near zero [see Fig. 8(c)]. The feature appearing only in quenches from the anisotropic boundary is that at DQPT, the effects of cross-direction correlation functions reach their extrema [Figs. 8(c) and 8(d)], which differs from all other quenches studied.

The squeezing angle dynamics shown in Figs. 9(a) and 9(b) are similar to the quenches between Ising phases, where the squeezing vector rotates in the clockwise direction at the beginning and the decrease of the squeezing angles α_s is the most rapid at DQPT. In between the first and the second critical times, the squeezing vector turns its rotation direction and the increase in α_s is the fastest at the second critical time. On the other hand, the squeezing angle evolution for quenches from the anisotropic boundary [Figs. 9(c) and 9(d)] reaches its minimum at DQPT, marking the distinction from
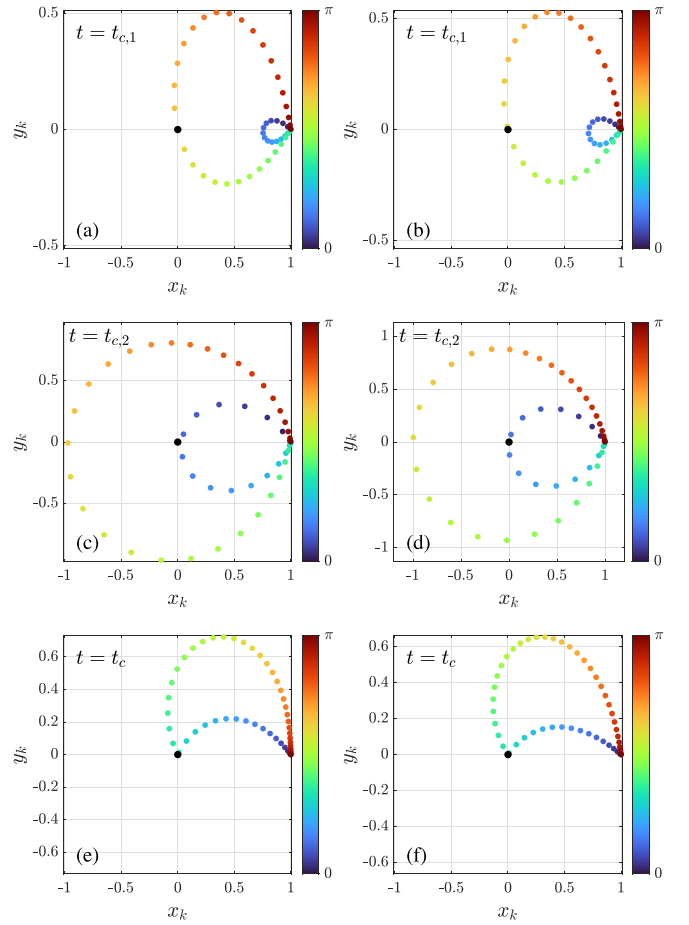

FIG. 7. Trajectories of $\vec{r}_k$'s at the critical times: (a), (c) upward quench [Fig. 6(a)]; (b), (d) downward quench [Fig. 6(b)]; quenches from anisotropic boundary to (e) FM$_x$ [Fig. 6(c)]; and (f) FM$_y$ [Fig. 6(d)] phase. Black dots indicate the origin at which the vectors are located. The color scale shows the progression of $\vec{r}_k$'s from $k = 0$ to π.

the cross-boundary quench cases. Then the whole evolution pattern follows what backward quenches have in Ising phases, where it oscillates around $\pi/2$ or π and never turns a full round.

C. Quenches from multicritical point

We study two cases when quenched from the multicritical point $(\delta_i, g_i) = (0, 1)$. Figure 10 shows the Loschmidt rate and spin-squeezing parameter evolutions. Notice the perfect oscillation of both LR and SSP for quench to $(\delta_f, g_f) = (1, 0)$, the case of a classical Ising model, in Fig. 10(a). The periodicity of SSP is half the periodicity of LR. This can be understood from the exact expressions of the LR and SSP; namely the LR is of the form

$$\lambda(t) = \tfrac{1}{2} \ln 8 - \tfrac{1}{4} \ln[38 + 24\cos(2t) + 2\cos(4t)] \quad (18)$$

and the SSP

$$\xi_S^2(t) = \frac{1}{8}\left[9 - \cos(4t) - \frac{1}{\sqrt{2}}\sqrt{\cos(8t) - 68\cos(4t) + 67} \right].$$
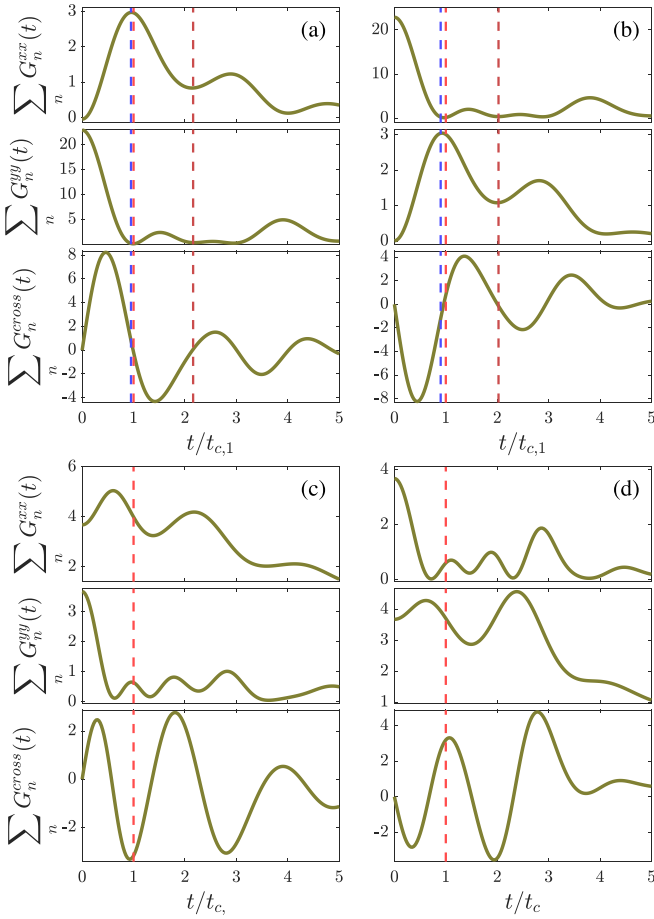$$(19)$$

FIG. 8. Scaled time plots of sums of correlation functions $G_n^{xx}(t)$ (top panels), $G_n^{yy}(t)$ (middle panels), and $G_n^{\mathrm{cross}}(t)$ (bottom panels) for the same quench cases as in Fig. 6. Red and blue dashed lines indicate the first peak of LRs and SSPs, respectively. The second red dashed lines in (a) and (b) represent the second critical time $t_{c,2}$ for each quench.

The half periodicity of SSP comes from the dominating $\cos(4t)$ term in SSP as compared to the dominating $\cos(2t)$ term in LR in Eqs. (18) and (19), respectively.

From Eq. (18), we see that the LR is independent of the system size N. The size independence also holds for SSP due to there being only a few nonzero correlation functions as follows:

$$G_2^{yy}(t) = G_{N-2}^{yy}(t) = \frac{1}{16}\sin^2(2t),$$

$$G_1^{xy}(t) = G_{N-1}^{xy}(t) = G_1^{yx}(t) = G_{N-1}^{yx}(t) = \frac{1}{8}\sin(2t), \quad (20)$$

and all other correlation functions vanish. In other words, in this quench case, all parallel-spin correlations along x are zero, whereas the next-nearest-neighbor correlations along y are finite, resulting in the summed correlation functions in Fig. 12(a). The observation here is counterintuitive to the fact that the system is quenched to the point where the y-direction interaction terms are less involved. Notice however that at DQPT, the $G_n^{yy}(t)$'s drop to zero as expected.

The aforementioned perfect pattern in the LR and SSP evolutions is destroyed when (δ_f, g_f) differs from the classical Ising model. As shown in Fig. 10(b), the SSP evolution is
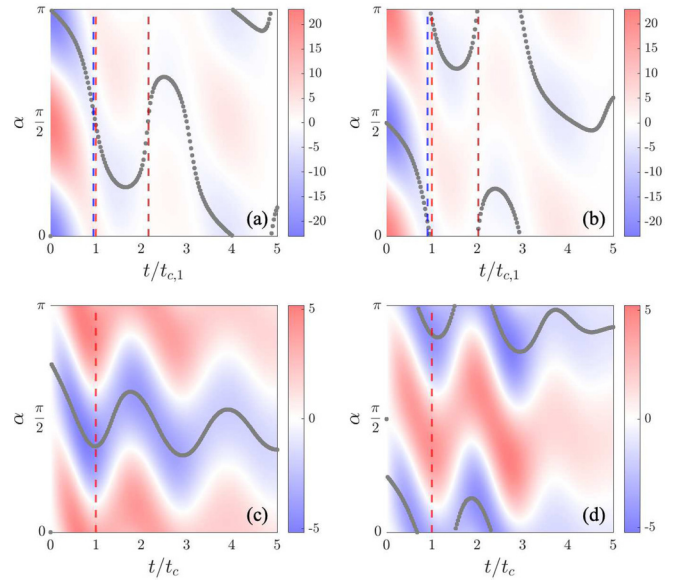

FIG. 9. Color map of $J(\alpha, t)$ for the same quench cases as in Fig. 6. Gray dots emphasize the squeezing angle α_s. Red and blue dashed lines refer to the first peak of LRs and SSPs, respectively. The second red dashed lines in (a) and (b) represent the second critical time $t_{c,2}$ for each quench.

distorted and resembles the pattern for a backward quench between Ising phases described in Sec. III A. It has twice as many peaks as the LR, and the major peaks occur near the respective critical times. Nevertheless, for both quench scenarios here, although they start from a critical point, the DTOPs show integer jumps, aligning with the case of quenches across the phase boundary instead of that from phase boundaries presented in the previous sections. The trajectories of the vectors $\vec{r}_k(t)$ are also similar to the quenches across the phase boundary (Fig. 11).

The sums of the time evolution of the correlation functions for the quench to (δ_f, g_f) that differs from the classical Ising model are shown in Fig. 12(b). The distortion emerges and the x-direction correlations rise a brief moment and then slowly decrease around DQPT. The perfect oscillation pattern of yy-correlation functions is deformed and interestingly they
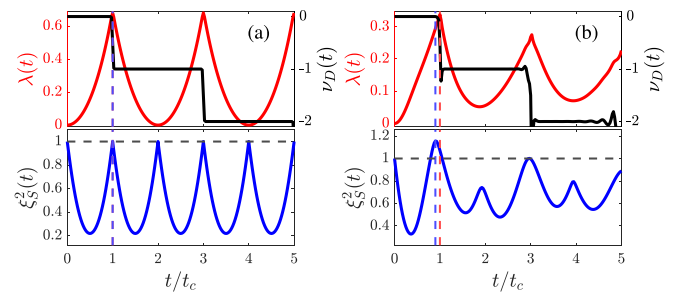

FIG. 10. Scaled time plots of LR, DTOP (top panels), and SSP (bottom panels) for (a) $(\delta_i, g_i) = (0, 1) \rightarrow (\delta_f, g_f) = (1, 0)$ and (b) $(\delta_i, g_i) = (0, 1) \rightarrow (\delta_f, g_f) = (0.5, 0.5)$. Red and blue dashed lines indicate the first peak of LRs and SSPs, respectively, and the two lines overlap with each other in (a). Black dashed horizontal lines indicate $\xi_S^2(t) = 1$.
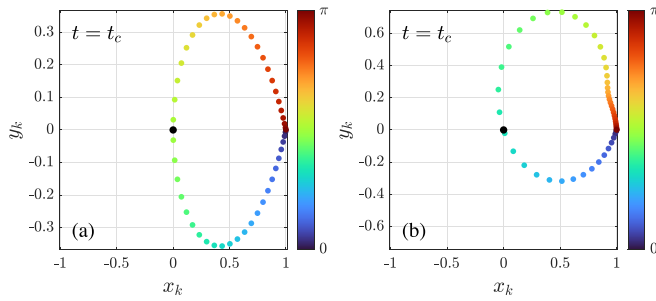
FIG. 11. Trajectories of $\vec{r}_k$'s at the corresponding critical times for the same quench cases as in Fig. 10. Black dots indicate the origin at which the vectors are located. The color scale shows the progression of $\vec{r}_k$'s from $k = 0$ to π.

FIG. 13. Color map of $J(\alpha, t)$ for the same quench cases as in Fig. 10. Gray dots emphasize the spin squeezing angle α_s. Red and blue dashed lines refer to the first peak of LRs and SSPs, respectively.

surpass the *xx*-correlation functions at the first critical time. On the other hand, the contribution of cross-spin correlations mostly vanishes at DQPT, while before and after DQPT they are of different signs, which resembles the quenches across the critical boundary to the FM_x phase.

In terms of the squeezing angle, the quench $(0, 1) \to (1, 0)$ acts like the limiting case of backward quenches between Ising phases shown in Fig. 5, where in Fig. 13(a) the slope of the squeezing angle approaches $-\infty$ at the first DQPT. The squeezing vector never completes a full rotation; rather it zigzags between the fourth and the first quadrants, i.e., $\alpha_s \in [3\pi/4, \pi)$ in $0 < t < t_c$ and $\alpha_s \in (0, \pi/4]$ in $t_c < t < 2t_c$. Note that in the evolution of α_s for the case shown in Fig. 13(b), the squeezing vector rotates anticlockwise and completes a full circle for one revival time. Again we observe the same phenomenon that the change of α_s is the maximum at DQPT.

IV. DISCUSSION

In the previous section, we showed that the time evolution of the correlation functions matches the physical properties of
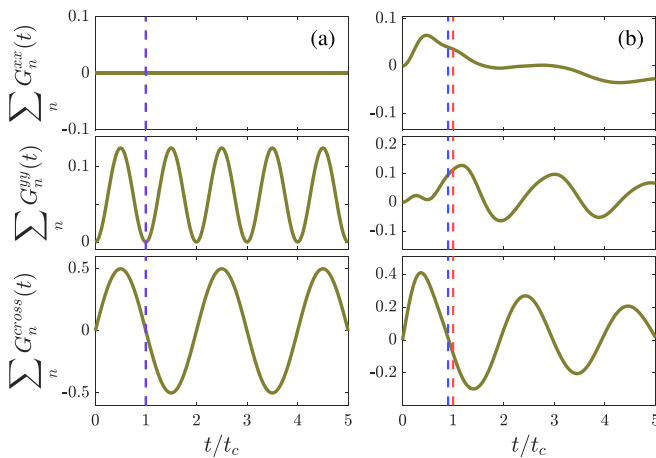

FIG. 12. Scaled time plots of sums of correlation functions $G_n^{xx}(t)$ (top panels), $G_n^{yy}(t)$ (middle panels), and $G_n^{cross}(t)$ (bottom panels) for the same quench cases as in Fig. 10. Red and blue dashed lines indicate the first peak of LRs and SSPs, respectively, and the two lines overlap with each other in (a).
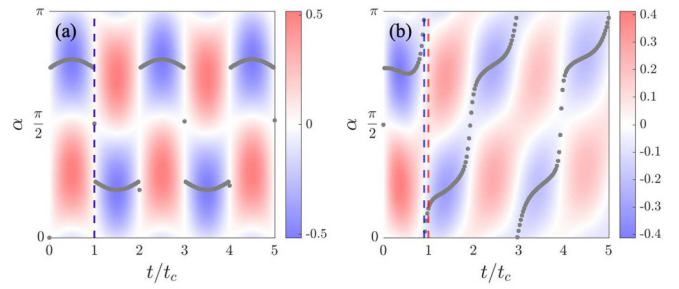
the phase that one quenches to in most of the cases. Here we provide an insight for the whole quench dynamics of an interacting spin model: Once the system is being quenched, the cross-direction correlations begin either growing or shrinking for around half the critical time for all kinds of quench. At the same time for quenches between FM_x and FM_y phases, the parallel-spin correlations evolve according to what phase the system is quenched to: when the final phase is flavored *x* spin, the $G_n^{xx}(t)$'s grow, whereas when the final phase is flavored *y* spin, the $G_n^{yy}(t)$'s grow. In the vicinity before the first DQPT, the flavoring parallel-spin correlation functions reach their maximal values while the contribution of cross-spin correlations diminishes. In this sense, the system does appear to "transit" to the final phase at DQPT for a brief amount of time. For the case of quenching to PM phase, interestingly, the supposedly low *yy*-spin correlations rise and peak just before DQPT. However, the originally flavored *xx*-spin correlations shrink to near minimum. This serves as evidence of "leaving" the original phase. On the other hand, the cross-spin correlation functions rarely play a role during DQPT caused by quenching across the critical boundary, but they do contribute for quenches from critical boundaries, especially for the quench from the anisotropic boundary, where the cross-spin correlations contribute a big part in minimizing SSP around DQPT.

Following this interpretation, perhaps we can provide crucial evidence suggesting the second DQPT for quenches across the anisotropic boundary is more of a "partial return transition" to the initial state. Namely, Figs. 7(a)–7(d) show that the trajectory of the loops including k_1^* (red loop) and k_2^* (blue loop) progresses in opposite direction. The strongest evidence comes from the sums of correlation functions in Figs. 8(a) and 8(b). In the summed $G_n^{xx}(t)$ and summed $G_n^{yy}(t)$ plots, the first DQPTs occur when the corresponding flavoring correlations of the postquenched Hamiltonian peak, while at the second critical time $t_{c,2}$ these correlations become the lowest. On the contrary, the originally flavored correlations do not restore their domination, yet the nearest-neighbor as well as the first few *n* correlations do rise and peak before the second DQPT, as shown in Fig. 14, making the summed quantities rise a little between the two critical times. The cross-spin correlation functions vanish as expected for DQPTs. The evolution of the squeezing angles also strengthens the argument, where the squeezing vectors change their rotation directions after $t_{c,1}$ and the squeezing angles pass through $t_{c,2}$ with the
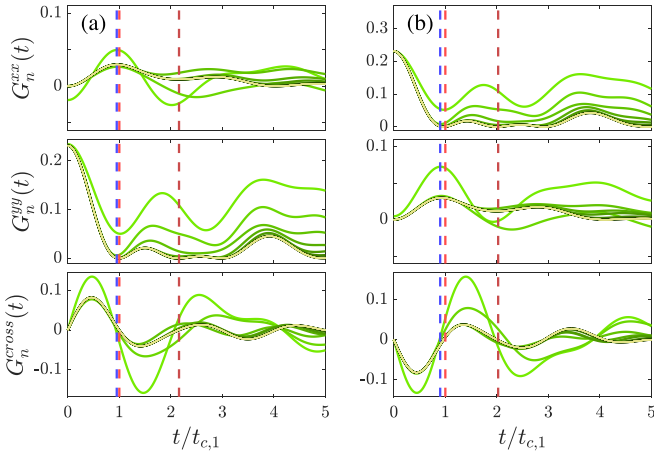
FIG. 14. Correlation functions for quenches across anisotropic boundary: (a) $(-1.2, 0.5) \rightarrow (0.8, 0.5)$ and (b) $(0.8, 0.5) \rightarrow (-0.8, 0.5)$. We show here $n \leqslant 10$ from light green to dark green with increasing n. Correlations for larger n's converge to the curve in yellow. The first and the second red dashed lines indicate $t_{c,1}$ and $t_{c,2}$, respectively. Blue dashed lines represents the maximum of SSPs.

greatest slope. After $t_{c,2}$, the squeezing vectors return back to the original rotation direction to complete a full turn. In short, the above evidence suggests the system may partially and temporarily return to a state having the spin character of the initial state in the vicinity of the second DQPT.

In studying the dynamics around DQPT, often the time-evolved SSP peaks around the critical time. This implies the system is the least squeezed around DQPT. Here we exploit some possible reasons behind regarding the first critical time. From the analytical expression of the SSP in Eq. (14), peaked SSP occurs when $G_n^{xx}(t) + G_n^{yy}(t)$ is high and $G_n^{xx}(t) - G_n^{yy}(t)$ and $G_n^{\mathrm{cross}}(t)$ are minimal. We can immediately see that for all the quench cases we studied, except quenches from phase boundary to the ordered phase, the cross-spin correlation functions are near zero, and the difference of x correlations and y correlations is minimized. This gives a small square-root term in Eq. (14) around DQPT and thus a relatively high SSP. In some cases like the backward quenches in Ising phases and quenches from the multicritical point, some $G_n^{yy}(t)$'s are negative in the transient regime, plus there is the growing contribution from $G_n^{\mathrm{cross}}(t)$; the SSP in these cases drops at the beginning. Shortly after, the quantities get lowered to minimal and thus SSPs grow to their maxima near critical time. To put it more generally, when quenched from some phase to the FM_x phase, the sums of $G_n^{xx}(t)$'s are around their maxima and sums of $G_n^{xx}(t)$'s would behave such that $G_n^{xx}(t) - G_n^{yy}(t)$ is low at DQPT. The opposite is true for quenches to the FM_y phase. In other words, the x and y spins are of the most uncertain around DQPT. The cross-spin correlations behave in such a way that they vanish at DQPT while before and after DQPT they evolve in opposite sign, making the SSP away from critical time drops.

Besides the different evolutions of spin-related quantities, the overall spin dynamics relating to the types of quenches within one quench scenario is also studied and we found a general relationship between cases with and without successful DQPTs as well as the critical spin dynamics around the
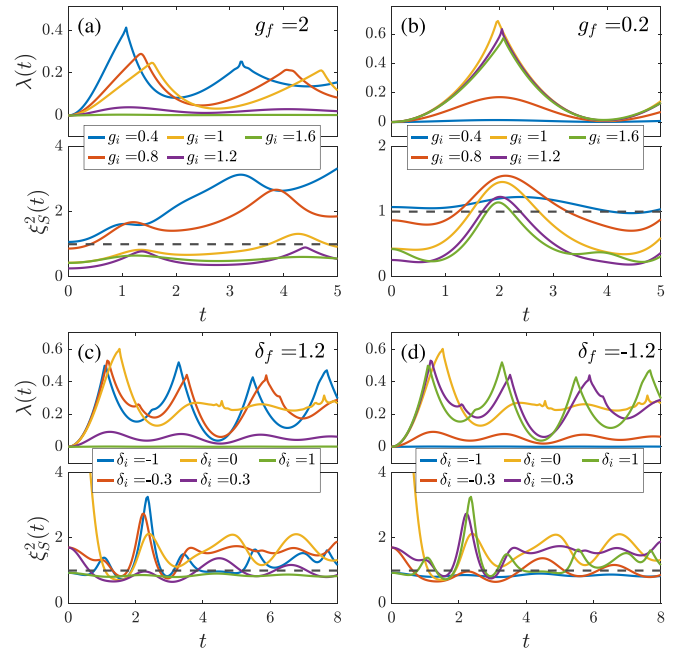

FIG. 15. LR and SSP plots of (a), (b) quenches across Ising boundary for fixed g_f with $\delta = 0.8$ and (c), (d) quenches across anisotropic boundary with fixed δ_f with $g = 0.5$. Black dashed lines indicate the line where $\xi_S^2(t) = 1$.

first critical time. In Fig. 15, we plot the rate functions and spin-squeezing parameters for quenches starting from various points in the equilibrium phase diagram. The case involving Ising phases shows an apparent distinction from quenches across the critical point and within one phase. Namely, SSPs are generally high and growing for forward quenches, while low and oscillating below 1 mostly for backward quenches. Quenches within one phase, on the other hand, evolve below 1 for forward quenches and above 1 for backward quenches. The case when the initial point is at the critical point behaves between the two, where the SSP oscillates around 1. Special features can also be observed during successful DQPTs for quenches across the anisotropic boundary. In Figs. 15(c) and 15(d), quenches across the critical point result in a sharp peak in SSP at the two critical times, while those peaks are absent in quenches within one phase where no DQPT occurs. Also for the quenches within the phase, the SSPs evolve around and below 1. The critical quench, on the other hand, differs drastically from other cases, where the SSP falls from infinity to a minimum at DQPT, as stated in Sec. III B. In either case, we further confirm the phenomenon that SSP reaches its local extremum (usually maximum) when approaching DQPT.

V. CONCLUSION

We analyzed three distinct quench scenarios in the XY model, for which we successfully detected some physical properties that an integrable spin-$\frac{1}{2}$ model might have when quenched between different phases. First, the collective spin of the system tends to fluctuate more when approaching critical times. This can be observed by the time evolution

of the spin-squeezing parameter of the system; namely the SSP peaks, or the system is the least spin-squeezed, just before DQPT occurs. This phenomenon seems to persist for longer critical times and for most types of quenches—whether quenched across or from critical boundaries, except when the system is initially in the most unsqueezed state where the SSP diverges. In either case, the system exhibits extreme spin-squeezing dynamics relative to the initial state, being the least or the most spin-squeezed situation, in the vicinity of DQPTs.

By observing the exact analytical expressions for the time evolution of the spin-squeezing parameter, we also reveal the spin dynamics by studying the competition between parallel- and cross-spin correlations. We find that during DQPTs, the system does appear to evolve in such a way to match the spin properties of the phase one quenches to. For instance, when quenched to xx-spin-flavored phase, the x-direction correlation grows to its maximum at DQPTs. This maximum reflects that the system is in the least unsqueezed state during DQPTs. Furthermore, we also showed that there is possibly some kind of "return transition" occurring for models having two critical momenta during the second DQPTs.

In short, the time evolution of SSP provides us nontrivial physical insights into the spin correlations around DQPTs,

though we would like to remark that the SSP is not a precise order parameter of DQPTs and this work is not intended to address whether the spin correlations are the driver of DQPTs. Nevertheless, the above-mentioned observations welcome further confirmation in experiments, and in other models, for example, the long-range transverse-field Ising model and the Lipkin-Meshhov-Glick model, which have been extensively studied for their intriguing dynamical behaviors around various types of phase transitions [5,51,71,72]. It will be interesting to understand the role of long-range interactions in the spin correlation dynamics and the relation to DQPTs. Moreover, the period halving in the SSP peaks relative to the LR observed in some cases would also serve as an interesting future work on how the quenched phases might affect the evolution of spin correlations.

[1] M. Heyl, A. Polkovnikov, and S. Kehrein, Phys. Rev. Lett. **110**, 135704 (2013).

[2] M. Heyl, Rep. Prog. Phys. **81**, 054001 (2018).

[3] A. A. Zvyagin, Low Temp. Phys. **42**, 971 (2016).

[4] B. Žunkovič, M. Heyl, M. Knap, and A. Silva, Phys. Rev. Lett. **120**, 130601 (2018).

[5] J. C. Halimeh and V. Zauner-Stauber, Phys. Rev. B **96**, 134427 (2017).

[6] E. A. Yuzbashyan, O. Tsyplyatyev, and B. L. Altshuler, Phys. Rev. Lett. **96**, 097005 (2006).

[7] B. Sciolla and G. Biroli, Phys. Rev. Lett. **105**, 220401 (2010).

[8] B. Žunkovič, A. Silva, and M. Fabrizio, Phil. Trans. R. Soc. A **374**, 20150160 (2016).

[9] T. Tian, Y. Ke, L. Zhang, S. Lin, Z. Shi, P. Huang, C. Lee, and J. Du, Phys. Rev. B **100**, 024310 (2019).

[10] P. Jurcevic, H. Shen, P. Hauke, C. Maier, T. Brydges, C. Hempel, B. P. Lanyon, M. Heyl, R. Blatt, and C. F. Roos, Phys. Rev. Lett. **119**, 080501 (2017).

[11] J. Zhang, G. Pagano, P. W. Hess, A. Kyprianidis, P. becker, H. Kaplan, A. V. Gorshkov, Z.-X. Gong, and C. Monroe, Nature (London) **551**, 601 (2017).

[12] N. Fläschner, D. Vogel, M. Tarnowski, B. S. Rem, D.-S. Lühmann, M. Heyl, J. C. Budich, L. Mathey, K. Sengstock, and C. Weitenberg, Nat. Phys. **14**, 265 (2018).

[13] X.-Y. Guo, C. Yang, Y. Zeng, Y. Peng, H.-K. Li, H. Deng, Y.-R. Jin, Sh. Chen, D. Zheng, and H. Fan, Phys. Rev. Appl. **11**, 044080 (2019).

[14] H.-X. Yang, T. Tian, Y.-B. Yang, L.-Y. Qiu, H.-Y. Liang, A.-J. Chu, C. B. Dağ, Y. Xu, Y. Liu, and L.-M. Duan, Phys. Rev. A **100**, 013622 (2019).

[15] T. Tian, H.-X. Yang, L.-Y. Qiu, H.-Y. Liang, Y.-B. Yang, Y. Xu, and L.-M. Duan, Phys. Rev. Lett. **124**, 043001 (2020).

[16] K. Xu, Z.-H. Sun, W. Liu, Y.-R. Zhang, H. Li, H. Dong, W. Ren, P. Zhang, F. Nori, D. Zheng, H. Fan, and H. Wang, Sci. Adv. **6**, eaba4935 (2020).

[17] H. Bernien, S. Schwartz, A. Keesling, H. Levine, A. Omran, H. Pichler, S. Choi, A. S. Zibrov, M. Endres, M. Greiner, V. Vuletić, and M. D. Lukin, Nature (London) **551**, 579 (2017).

[18] E. Guardado-Sanchez, P. T. Brown, D. Mitra, T. Devakul, D. A. Huse, P. Schauss, and W. S. Bakr, Phys. Rev. X **8**, 021069 (2018).

[19] M. Heyl, Phys. Rev. Lett. **115**, 140602 (2015).

[20] M. Heyl, Phys. Rev. Lett. **113**, 205701 (2014).

[21] S. A. Weidinger, M. Heyl, A. Silva, and M. Knap, Phys. Rev. B **96**, 134313 (2017).

[22] P. Titum, J. T. Iosue, J. R. Garrison, A. V. Gorshkov, and Z.-X. Gong, Phys. Rev. Lett. **123**, 115701 (2019).

[23] R. Jafari, Sci. Rep. **9**, 2871 (2019).

[24] M. Schmitt, and S. Kehrein, Phys. Rev. B **92**, 075114 (2015).

[25] M. Schmitt and M. Heyl, SciPost Phys. **4**, 013 (2018).

[26] G. Torlai, L. Tagliacozzo, and G. D. Chiara, J. Stat. Mech. (2014) P06001.

[27] E. Canovi, E. Ercolessi, P. Naldesi, L. Taddia, and D. Vodola, Phys. Rev. B **89**, 104303 (2014).

[28] N. Sedlmayr, P. Jaeger, M. Maiti, and J. Sirker, Phys. Rev. B **97**, 064304 (2018).

[29] K. Pöyhönen and T. Ojanen, Phys. Rev. Res. **3**, L042027 (2021).

[30] R. Vosk and E. Altman, Phys. Rev. Lett. **112**, 217204 (2014).

[31] A. Patra, V. Mukherjee, and A. Dutta, J. Phys.: Conf. Ser. **297**, 012008 (2011).

[32] S. De Nicola, B. Doyon, and M. J. Bhaseen, J. Stat. Mech. (2020) 013106.

[33] S. De Nicola, A. A. Michailidis, and M. Serbyn, Phys. Rev. Lett. **126**, 040602 (2021).

[34] M. Heyl, F. Pollmann, and B. Dóra, Phys. Rev. Lett. **121**, 016801 (2018).

[35] J. C. Budich and M. Heyl, Phys. Rev. B **93**, 085416 (2016).

[36] W. C. Yu, P. D. Sacramento, Y. C. Li, and H.-Q. Lin, Phys. Rev. B **104**, 085104 (2021).

[37] T. V. Zache, N. Mueller, J. T. Schneider, F. Jendrzejewski, J. Berges, and P. Hauke, Phys. Rev. Lett. **122**, 050403 (2019).

[38] S. Vajna and B. Dóra, Phys. Rev. B **89**, 161105(R) (2014).

[39] M. Lacki and M. Heyl, Phys. Rev. B **99**, 121107(R) (2019).

[40] A. Lahiri and S. Bera, Phys. Rev. B **99**, 174311 (2019).

[41] K. Yang, L. Zhou, W. Ma, X. Kong, P. Wang, X. Qin, X. Rong, Y. Wang, F. Shi, J. Gong, and J. Du, Phys. Rev. B **100**, 085308 (2019).

[42] A. Kosior and K. Sacha, Phys. Rev. A **97**, 053621 (2018).

[43] T. H. Kyaw, V. M. Bastidas, J. Tangpanitanon, G. Romero, and L. C. Kwek, Phys. Rev. A **101**, 012111 (2020).

[44] A. A. Zvyagin, Phys. Rev. B **95**, 075122 (2017).

[45] R. Jafari, H. Johannesson, A. Langari, and M. A. Martin-Delgado, Phys. Rev. B **99**, 054302 (2019).

[46] R. Jafari and A. Akbari, Phys. Rev. A **103**, 012204 (2021).

[47] S. Zamani, R. Jafari, and A. Langari, Phys. Rev. B **102**, 144306 (2020).

[48] S. Bandyopadhyay, A. Polkovnikov, and A. Dutta, Phys. Rev. Lett. **126**, 200602 (2021).

[49] J. C. Halimeh, D. Trapin, M. VanDamme, and M. Heyl, Phys. Rev. B **104**, 075130 (2021).

[50] O. N. Kuliashov, A. A. Markov, and A. N. Rubtsov, Phys. Rev. B **107**, 094304 (2021).

[51] I. Homrighausen, N. O. Abeling, V. Zauner-Stauber, and J. C. Halimeh, Phys. Rev. B **96**, 104436 (2017).

[52] C. Ding, Phys. Rev. B **102**, 060409(R) (2020).

[53] C. Karrasch and D. Schuricht, Phys. Rev. B **87**, 195104 (2013).

[54] J. N. Kriel, C. Karrasch, and S. Kehrein, Phys. Rev. B **90**, 125106 (2014).

[55] H. Cheraghi, M. J. Tafreshi, and S. Mahdavifar, J. Magn. Magn. Mater. **497**, 166078 (2020).

[56] D. M. Kennes, D. Schuricht, and C. Karrasch, Phys. Rev. B **97**, 184302 (2018).

[57] K. Seetharam, Y. Shchadilova, F. Grusdt, M. B. Zvonarev, and E. Demler, Phys. Rev. Lett. **127**, 185302 (2021).

[58] M. Sadrzadeh, R. Jafari, and A. Langari, Phys. Rev. B **103**, 144305 (2021).

[59] J. Naji, M. Jafari, R. Jafari, and A. Akbari, Phys. Rev. A **105**, 022220 (2022).

[60] R. Jafari, A. Akbari, U. Mishra, and H. Johannesson, Phys. Rev. B **105**, 094311 (2022).

[61] U. Mishra, R. Jafari, and A. Akbari, J. Phys. A: Math. Theor. **53**, 375301 (2020).

[62] J. C. Halimeh, M. Van Damme, V. Zauner-Stauber, and L. Vanderstraeten, Phys. Rev. Res. **2**, 033111 (2020).

[63] T. Hashizume, Ian P. McCulloch, and J. C. Halimeh, Phys. Rev. Res. **4**, 013250 (2022).

[64] M. Van Damme, T. V. Zache, D. Banerjee, P. Hauke, and J. C. Halimeh, Phys. Rev. B **106**, 245110 (2022).

[65] P. Uhrich, N. Defenu, R. Jafari, and J. C. Halimeh, Phys. Rev. B **101**, 245148 (2020).

[66] J. Lang, B. Frank, and J. C. Halimeh, Phys. Rev. Lett. **121**, 130603 (2018).

[67] F. Andraschko and J. Sirker, Phys. Rev. B **89**, 125120 (2014).

[68] S. Morrison and A. S. Parkins, Phys. Rev. Lett. **100**, 040403 (2008).

[69] S. Porta, F. Cavaliere, M. Sassetti, and N. T. Ziani, Sci. Rep. **10**, 12766 (2020).

[70] C. Y. Wong and W. C. Yu, Phys. Rev. B **105**, 174307 (2022).

[71] À. L. Corps and A. Relaño, Phys. Rev. B **106**, 024311 (2022).

[72] À. L. Corps and A. Relaño, Phys. Rev. Lett. **130**, 100402 (2023).

[73] J. Ma, X. Wang, C. P. Sun, and F. Nori, Phys. Rep. **509**, 89 (2011).

[74] C. Gross, J. Phys. B: At. Mol. Opt. Phys. **45**, 103001 (2012).

[75] L. Pezzè, A. Smerzi, M. K. Oberthaler, R. Schmied, and P. Treutlein, Rev. Mod. Phys. **90**, 035005 (2018).

[76] C. D. Hamley, C. S. Gerving, T. M. Hoang, E. M. Bookjans, and M. S. Chapman, Nat. Phys. **8**, 305 (2012).

[77] Z. Sun, Phys. Rev. A **84**, 052307 (2011).

[78] J. Vidal, G. Palacios, and R. Mosseri, Phys. Rev. A **69**, 022107 (2004).

[79] Y. Huang, Y. Ding, J. Xu, J. Liu, H. Wang, and H.-N. Xiong, Phys. Rev. A **106**, 022430 (2022).

[80] H. Cheraghi, S. Mahdavifar, and H. Johannesson, Phys. Rev. B **105**, 024425 (2022).

[81] M. Kitagawa and M. Ueda, Phys. Rev. A **47**, 5138 (1993).

[82] S. Sachdev, *Quantum Phase Transitions* (Cambridge University Press, Cambridge, 1999).

[83] E. Barouch, B. M. McCoy, and M. Dresden, Phys. Rev. A **2**, 1075 (1970).

[84] E. Barouch and B. M. McCoy, Phys. Rev. A **3**, 786 (1971).

[85] S. Pancharatnam, Proc. Indian Acad. Sci. A **44**, 247 (1956).

[86] J. Samuel and R. Bhandari, Phys. Rev. Lett. **60**, 2339 (1988).

[87] G.-R. Jin and S. W. Kim, Phys. Rev. A **76**, 043621 (2007).

[88] E. Lieb, T. Schultz, and D. Mattis, Ann. Phys. **16**, 407 (1961).